Effective conductivity measurement of CNT/Polymer films using a non-contact microwave technique

Nacer Badi[1,2,*], Rakesh Mekala[3], Dhivya Ketharnath[3], Francisco Robles Hernandez[4], and Jarek Wosik[3,5]

[1]Center for Advanced Materials, University of Houston, Houston, TX77204-5004
[2]Department of Physics, University of Houston, Houston, TX77204-5005
[3] Electrical & Computer Engineering, University of Houston, Houston, TX 77204-4005
[4]College of Engineering Technology, University of Houston, Houston, TX 77204-4020
[5]Texas Center for Superconductivity, University of Houston, Houston, TX, 77204-5002

Fairouz Chouit, Skander Boukhezar, Ouanassa Guellati, and Mohamed Guerioune

Laboratory LEREC, Department of Physics, University of Annaba, Algeria, BP12 - 23000

*E-mail address of corresponding author, nbadi@uh.edu Phone: 713 743-3621

ABSTRACT

Carbon nanotubes (CNTs) have recently been utilized to improve the mechanical and heat transfer characteristics, electromagnetic shielding, and to enhance the electrical conductivity of the resulting composites. CNT reinforced composites have applications in electronics, optoelectronics, photovoltaic, sensors, structural materials, and energy storage systems. Electrical characteristics, such as alternating current (AC) complex conductivity and dielectric permittivity are key functional parameters of these materials. Measurement methods need to be optimized to obtain data to further enhance the quality control and manufacturing process.

This paper reports on successful synthesis of pristine CNT materials and HDPE/CNTs composites by catalytic chemical vapor deposition (CCVD) and melt processing techniques, respectively. This includes CNT/composite samples produced by uniform dispersion of up to 1% of MWCNTs in Grade TR144 HDPE polymer matrix. Elaborated samples were subjected to structural characterizations and complex conductivity measurements under single post dielectric resonator (SPDR) operating at 13 GHz. Results on complex conductivity properties of composite materials with specific emphasis on reflected and transmitted non-contact microwave measurements are presented and discussed.

***Keywords*:** CNT/polymer composites, complex conductivity, dielectric permittivity, percolation network, non-contact microwave measurement.

1.0 INTRODUCTION

Nanocomposites based on carbon nanotubes (CNTs) are a very active area of research as they exhibit several new properties and functions, compared with pure CNTs. Depending upon the nature of applications, such CNT-nanocomposites can be fabricated with polymers, which are normally electrically insulating, flexible, have low density and are easily prepared and mixed with CNTs, which have excellent electrical conductivity, extra mechanical strength and high thermal conductivity. It has been reported that these nanocomposites materials have shown highly useful electromagnetic shielding characteristics as the electrical conductivity and dielectric losses can be tuned by varying the concentration and orientation of the nanotubes along with other fillers. In addition, these nanotubes can be subjected to a variety of treatment which can be applied to nanotubes either during or after fabrication to optimize their electrical properties. Teachings from the published literature [1,2] were used and applied to improve the electrical and microwave absorption properties of the proposed CNT-nanocomposites. In this work, the selectivity of microwave absorption of the fabricated samples was tuned by matching the dielectric loss and the conductivity loss via increasing the loading up to 1% of MWCNTs in Grade TR144 HDPE nanocomposites. By controlling these factors, the frequencies corresponding to the maximum loss can be tailored throughout the frequency range of operation. Theoretical analyses of the microwave interaction with investigated samples were performed using a commercial electromagnetic fields simulator (HFSS, Ansoft Inc.).

2.0 EXPERIMENTAL

2.1. CNTs synthesis

The nitrogen doped N-MWCNTs listed in Table 1 were synthesized by catalytic chemical vapor deposition (CCVD) using a mixture of C_2H_6/Ar/NH_3 on an alumina supported iron catalyst. The iron loading was set at 20 wt % using impregnating method. Nitrogen and carbon sources were provided by ammonia 50 ml/min (Air liquide, 99.9996%) and Ethane 50 ml/min (Linde, 99.9995%), respectively.

The as-synthesized N-MWCNTs at 850°C during 2h were treated in a soda solution at 110 °C for 24 h to dissolve residual alumina support. The solid was washed several times with deionized water until a neutral pH was reached. It was further treated with an aqua regia medium at 110°C for 17 h to remove the residual iron catalyst following by water washing to obtained about 3 wt.%.

Materials	Surface area (m^2/g)	N at.%	I_D/I_G
N-MWCNT with H_2	87	2.15 with much quaternary binding	1.14
N-NWCNT without H_2	80	1.97	1.37

Table.1: N-MWCNTs bamboo shape with 97% purity and high selectivity (~ 12 - 100 nm).

2.2. Nanocomposites Preparation

The polymer matrix used in this work is high density polyethylene (HDPE) resin with trade name TR144, it was supplied by Sonatrach company CP2K (Complexe Pétrolier de Skikda, Algeria). The melt index of HDPE pellets was 0.30 and had a density of 0.942-0.947 g/cm^3. HDPE/N-MWCNTs were prepared via the melt-compounding method using a twin screw mixer (Brabender), the manufacturing temperature was kept for 167°C and the screw speed amounted to 100 rpm for 10 min. The weight fractions of N-MWCNTs filler were fixed at 0.1, 0.4, 0.8 and 1wt%. The composite was then chopped into smaller pieces and putted in a mould of 50 x 70 x 0.5mm dimensions. This latter were then hot pressed at 177°C, under pressure of 100 bars for 5 min to obtain films. In addition, a sample of neat HDPE was similarly prepared as standard reference.

2.3. Samples characterization

a. Characterization of carbon nanotubes:

The morphology of the N-MWCNTs was examined by scanning electron microscopy (SEM) on a JEOL 6700-FEG microscope. Transmission electron microscopy (TEM) observations were carried out using a JEOL JEM-2010F under an accelerated voltage of 200 kV with a point-to-point resolution of 0.23 nm.

The combustion was made in an air atmosphere using a Q5000 apparatus (TA instrument), with a gas flow rate of 20 ml/min, until 1000°C at approximately 10°C/min. Raman spectroscopy was carried out on a Microraman RENISHAW spectrometer RAMASCOPE 2000 with a spot size of 1 μm^2 and 1 cm^{-1} resolution) working with a He–Ne Laser beam with 632.8 nm wavelength.

Specific surface area measurements were carried out on a Tristar (Micromeritics) sorptometer using nitrogen as adsorbent at liquid nitrogen temperature. Before measurements, the sample was outgassed at 250 ◦C for 3 h in order to desorb impurities and moisture from its surface. XPS analyses were performed with a MULTILAB 2000 (THERMO) spectrometer equipped with Al K_α anode (h_υ = 1486.6 eV) during 10 min of acquisition in order to achieve a good signal-to-noise ratio.

b. Microwave Characterization:

Microwave material characterization techniques have been used in a large number of applications and are classified as a nondestructive evaluation (NDE) method. Microwave techniques take advantage of the fact that in contrary to dc currents, *rf* currents cannot meander, thus the electromagnetic response is integrated over the whole volume where *rf* currents are induced and penetrate into the sample. At microwave frequencies dielectric resonators (DRs) are the preferred characterization tool over non-resonant methods due to their very high sensitivity (high quality-factors Q and very large dynamic range of measured resistance. There are many different versions of DRs where geometry and type of dielectric are designed and selected to efficiently/precisely analyze different materials [3].

In this work, we used single post dielectric resonator (SPDR) operating at 13 GHz in the $TE_{01\delta}$ mode as shown in Figure 1. The SPDR was designed for samples' placement in non-zero tangential electric field to ensure maximum measurement sensitivity of lossy and/or thin materials [4]. Its construction was similar to that used for measurements of the sheet resistance of graphene [5].

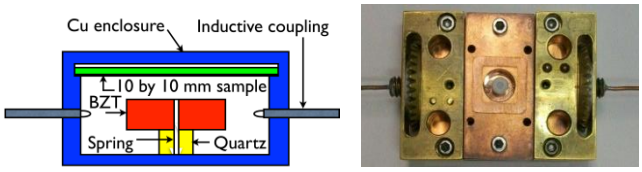

Fig.1. Schematic sketch and picture consisting of BZT dielectric, quartz support of the disk, copper enclosure and two coaxial coupling loops without upper cover.

The dielectric disk made from very low loss, temperature stable high-permittivity (ε_r = 27.93 at 300 K) barium zirconium titanate (BZT) ceramic ensures high Q-factor and thermal stability. The BZT dielectric of radius 2.5 mm and height 2 mm is placed in a copper enclosure of radius 9 mm. The BZT was placed 3 mm away from the copper enclosure by using a low loss quartz disk. The sample was placed at a distance of 2.5 mm from the dielectric disk. For the measurement of Q-factor and resonant frequency, the 10 mm x 10 mm samples are placed in the SPDR connected to the vector network analyzer for Q-factor measurements using the one-port

Kajfez method. The adjustable-insertion-coupling loop, which inductively excites the $TE_{01\delta}$ mode in the SPDR, was connected to the HP86390 network analyzer after calibration to remove the losses associated with the network analyzer cables.

3.0 RESULTS AND DISCUSSION

SEM and TEM micrographs in Fig. 2 were obtained to gain more information about the N-MWCNTs structures; they show the bamboo shape with 97% purity and high selectivity (~ 12 - 100 nm) with outer diameter around 40 nm [6,7]. The degree of nitrogen doping and the chemical bonding of the sample have been investigated by XPS spectroscopy which reveals the existence of C_{1s} and N_{1s} signals (not shown here). Furthermore, the N_{1s} XPS spectrum was de-convoluted into five to six peaks with principal binding energies at ~398, ~399 and ~ 401 eV, respectively, assigned to pyridine-like N, pyrrolic-like N and graphitic-like N [8]. Moreover, the binding energies at over 402 eV indicated the presence of N binding with oxygen groups.

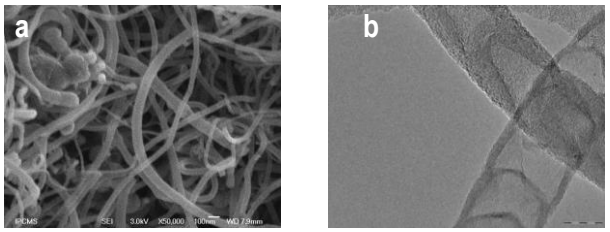

Fig. 2. SEM (a) and TEM (b) pictures of the N-MWCNTs

The Raman analysis for the composite is more complex and is presented in Figure 3. In this Figure can be observed the presence of the D and G bands in the background that is the result of the relatively low concentration of MWCNT added to the composite. However, for an addition of only 0.4 wt% of MWCNT is evident that the presence of the carbon nanostructures can be relatively easy detected. The D and G bands are located at similar bandwidth as the ones in the pristine material. What is of interest in this case is the presence of the 2D band that is clearly discernible in both composites. The 2D band is characteristics of the graphitic carbon and graphene structures. Possible that some of the carbon in the matrix is in the form of graphitic carbon or potentially is the result of the folded structures in the MWCNT that contribute to the presence of the 2D band [9,10].

On the other hand the larger intensity reflections are bands resulting from the HDPE used for the composite. The Raman spectrum corresponds to that reported previously in the literature for high density polyethylene [11]. The band at 1080 cm^{-1} is used to characterize the level of amorphous phase in the high density polyethylene. In fact Raman is one of the most powerful tools to characterize the crystallinity in high density polyethylene [11]. This is possible by measuring the intensity of the bands from 1400 to 1460 cm^{-1}. Those bands are characteristic of the methylene bending vibrations. In particular the band in the 1481 cm^{-1} region is typically assigned to that of the orthorhombic crystalline phase in polyethylene [11,12].

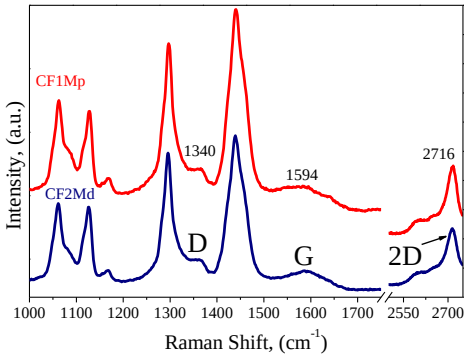

Fig.3. Raman Spectroscopy of MWCNT/HDPE composite.

Calculation and extraction of effective conductivity

Extraction of either conductivity or complex permittivity from measured Q-factor and frequency shift require calculations of the EM fields in the resonant structure. To achieve this, we performed numerical simulations of the resonant structure using HFSS [13], a finite element method (FEM) simulator.

The resonator geometry is built in accordance to the dimensions of the SPDR as described in the experimental setup. A coupling loop drawn to mimic the experimental coaxial cable loop used to inductively excite the $TE_{01\delta}$ mode in the SPDR. In this prelimnary approach, the sample is defined in HFSS through a sheet resistance value. In HFSS, the incident signal from the network analyzer is coupled to the SPDR via a waveport defined as the (coaxial cable) coupling loop. To ensure the accuracy of the simulation solution, the structure was finely meshed along the dielectric disk and sample regions. Two different analysis methods, Eigen and driven mode, were used to calculate the dependence of Q-factor and resonant frequency, respectively, on sheet resistance ($1/\sigma h$) (1/S) using the SPDR's experimentally measured resonant frequency as the starting point (Table 2).

Figure 4 shows the theoretical Q-factor of the resonator with a sample included, computed for a various values of conductance (10^{-5} to 10^{4}) S. Experimental points of Q-values measured for each sample are marked on the $Q(\sigma h)$ curve. Such procedure allowed us for determination of effective σ values for each sample under consideration.

Overall, samples CFMp show higher quality factor and the resonance frequency shift toward higher frequencies, which indicate an increased shielding ability. CFMd samples exhibited a clear dependence of both frequency and Q-factor on CNT concentration. Only CF_3Md was not fully giving consistent EM response. This may be

attributed to the non-uniformity and/or non-flatness of the sample. Also percolation threshold of carbon nanotubes needs to be investigated and correlated with measured electromagnetic response. Further studies of this subject are underway and their results will be presented at the conference.

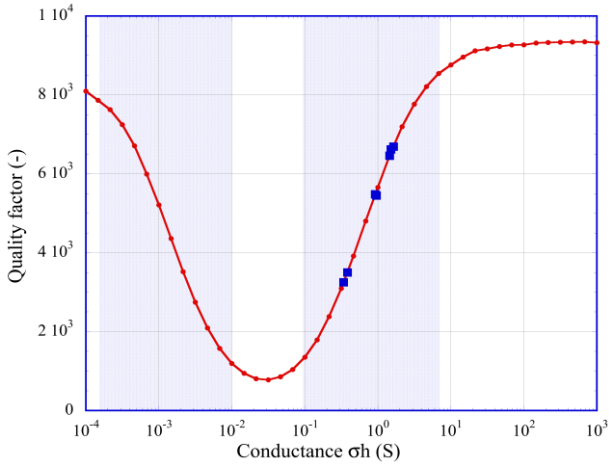

Fig.4. Correlated experimental data (blue square points) with Eigen mode calculations of Q-factor as a function of conductance (red circular points) for a BZT single post resonator.

Sample	MWNT (%)	$\Delta(\phi-f_{res})$ (MHz)	Q-factor (-)	Thickness (mm)	σh (S)	Effective σ (S/m)
HDPE	0	-9	3500	0.95	0.385	400.52
CF_1Md (H_2)	0.1	-6.9	5450	0.69	0.959	1389.8
$CF_2Md(H_2)$	0.4	9.9	6460	0.45	1.45	3222.22
$CF_3Md(H_2)$	0.8	-10.5	3250	0.89	0.34	382.0
$CF_4Md(H_2)$	1	6.3	5480	0.47	0.9205	1958.5
CF_1Mp	0.4	17.8	6620	0.32	1.513	4728.1
CF_2Mp	0.8	15.5	6690	0.35	1.643	4694.2

Table. 2. Q-factor and resonant frequency measurement using the $TE_{01\delta}$ mode 13 GHz BZT SPDR.

REFERENCES

[1] D.A. Usanov, A.V. Skripal and A.V. Romanov, "Complex permittivity of composites based on dielectric matrices with carbon nanotubes", Technical Physics, Vol. 56, No. 1, pp. 102-106, 2011.

[2] R. Fang,"Microwave Imaging Technology to Pinpoint Damage in Carbon nanotube Composites", Research Proposal, Institute of Biotechnology, University of Cambridge, May 2009.

[3] D. Kajfez, "Q-Factor," in Encyclopedia of RF and Microwave Engineering, ed: John Wiley & Sons, Inc., 2005.

[4] J. Krupka, J. Wosik, C. Jastrzebski, T. Ciuk, J. Mazierska, and M. Zdrojek, "Complex Conductivity of YBCO Films in Normal and Superconducting States Probed by Microwave Measurements," Applied Superconductivity, IEEE Transactions on, vol. 23, pp. 1501011-1501011, 2013.

[5] J. Krupka and W. Strupinski, "Measurements of the sheet resistance and conductivity of thin epitaxial graphene and SiC films," Applied Physics Letters, vol. 96, p. 082101, 2010.

[6]. Guellati O, Janowska I, Bégin D, Guerioune M, Mekhalif Z, Delhalle J, Moldovan S, Ersen O, Pham-Huu C, Applied Catalysis A: General 2012; 7:423– 424.

[7]. Chen L , Xia K , Huang L, Li L , Pei L , Fei S Facile synthesis and hydrogen storage application of nitrogen-doped carbon nanotubes with bamboo like structure, Int J Hydrogen Energy 2013;38: 3297-3303.

[8]. Wang C, Huang Z, Zhan L, Wang Y, Qiao W, Liang X, et al. Nitrogen-doped carbon nanotubes synthesized with carbon nanotubes as catalyst. Diam Relat Mater 2011;20:1353-6.

[9] A.E. Fals, V.G. Hadjiev, F.C.R. Hernández, Mater Chem Phys, In Press (2013).

[10] A.E. Fals, V.G. Hadjiev, F.C. Robles Hernández, Materials Science and Engineering: A, 558 (2012) 13-20.

[11] R.P. Paradkar, S.S. Sakhalkar, X. He, M.S. Ellison, J Appl Polym Sci, 88 (2003) 545-549.

[12] J.H. Schachtschneider, R.G. Snyder, Spectrochimica Acta, 19 (1963) 117-168.

[13] H. Ansoft, "ver. 12," Ansoft Corporation, Pittsburgh, PA, 2010.

ACKNOWLEDGMENTS

This material is based upon work supported by the Texas State Funds to the University of Houston Center for Advanced Materials (CAM) and the Texas Center for Superconductivity. LEREC thanks Sonatrach-CP2K for providing HDPE materials.